A METHOD FOR MODELLING OF CONTRAST ENHANCED MAMMOGRAPHY IMAGING: A SIMULATION STUDY

Tihomir Georgiev[1], Kristina Bliznakova[1], Yanka Baneva[2]

[1]*Department of Medical Equipment, Electronic and Information Technologies in Healthcare, Medical University – Varna*
[2]*Department of Physics and Biophysics, Medical University – Varna*

Abstract

Introduction: *Early detection of breast cancer is vital for many women. Mammography faces certain difficulties with dense breasts therefore a technique called contrast-enhanced dual-energy mammography (CEDEM) is used in such cases for small artefacts detection.*

Aim: *The aim of this study is to establish a framework of computational tools to design, simulate and investigate the CEDEM process.*

Materials and methods: *Two objects were created for this purpose, a parallelepiped with dimensions 75 mm x 60 mm x 50 mm with 10 pits on the top of it and a semi cylindrical shape for the second object 45 mm of height with 6 cylindrical cavities which differ in their height. Iohexol was used as a contrast media. The Beer's law was used for the simulation of the images, then noise was added, while series of coefficients were used to produce the subtraction result images.*

Results: *Good contrast of the subtracted images was achieved for low energy at 50 kVp and there was a negligible difference between theoretical and simulated weighted coefficients that provided best contrast.*

Conclusion: *The developed CEDEM framework will be used in optimising acquisition parameters for a range of specific cancerous cases.*

Keywords: *dual energy, noise simulation, radiology contrast*

Introduction

Risk from death from cancer varies between 7% and 13% for women in EU and the most diagnosed cancer type among women in every single European state is the breast cancer (1). Generally, according to American College of Radiology there are four types of BI-RADS® breasts composition categories from A to D respectively: almost entirely fatty, scattered areas of fibroglandular density, heterogeneously dense, and extremely dense (2). However, even the "gold standard" x-ray mammography imaging has certain difficulties to detect early cancer in above categories C and D; therefore, a more complicated method can be employed – images are taken using two different energy settings, which result in generation of low- and high- energy images. In some cases, a contrast agent is injected in advanced. The final image is obtained by applying a subtraction algorithm (3-5). This technique is called dual-energy mammography (DEM), while contrast-enhanced dual-energy mammography (CEDEM) is called the technique with the use of a contrast agent. The advantages in clinical application of CEDEM were easy implementation, application in some specific cases of lesions, and others as well as chemotherapy response (4).

Another technique that may provide even better results than CEDEM is the single-energy temporal subtraction (SETS) which uses a single energy spectrum and images are taken before and after injection of a contrast agent (3,4). However, it has the drawback that it is difficult to ensure the breast remains motionless for certain time period of several minutes after injection of the contrast agent (3,4) and therefore, additional processing has to be performed in order to eliminate the effects of motion (3) while CEDEM has also the advantage to allow for acquisition in different views (4).

A research study involving 120 patients (5) found that sensitivity for mammography and CEDEM together was higher than for mammography alone and no specificity loss, and both sensitivity and specificity for mammography and CEDEM together were not statistically different than those for mammography and ultrasound together. One more recent study with participants mostly with dense breasts (6) found CEDEM performed better than mammography in sensitivity although specificity was slightly less. Study, involving 251 participants, compared CEDEM with magnetic resonance imaging for detection of breast lesions and found the former to have higher specificity and positive predictive value (PPV), while sensitivity and negative predictive value (NPV) were reported comparable (7). The CEDEM technique can be used also to differentiate malignant from benign lesions. A study involving 593 lesions detected in 547 patients reported that use of CEDEM to classify lesion types resulted in sensitivity 97.86% and NPV 95.76%, however specificity was low – only 59.4% (8). In a retrospective study with 999 patients, digital mammography and contrast-enhanced dual-energy mammography were compared to determine multifocal-multicenter cancer against unifocal with cancers being confirmed by histopathology (9). The study reported that CEDEM had higher figures in sensitivity, NPV and accuracy.

Above studies revealed the potential advantages of the CEDEM. Further work is related to the optimization of both clinical protocols and the whole CEDEM imaging chain, which is best performed by using phantoms.

Specific computational phantoms to be used for contrast-enhanced clinical optimization studies were designed, then we simulated X-ray images by using an in-house software application, the images were modified to include photon noise, and then suitably processed to obtain CEDEM images. The evaluation included measurements of contrast.

Aim: The aim of this study is to establish a framework of computational tools to design, simulate and investigate the CEDEM process.

Materials and methods

Phantoms: We used in-house software application XRayImagingSimulator (10) to create two computational objects. The first object is a parallelepiped modelled from clear resin. Its dimensions were designed to be 75 mm x 60 mm x 50 mm with ten pits with a radius of 4 mm on the top of it. The pits depths are from 0.1 mm to 1.0 mm. The second object has a semi cylindrical shape with a radius of 50 mm and a height of 45 mm. Within this object, there are 6 cylindrical cavities, each of them with a radius of 10 mm and different heights – 2 mm, 3mm, 4 mm, 5 mm, 6 mm, 8 mm. The material for this second object was polymethyl methacrylate (PMMA). The background materials: clear resin and PMMA were selected as they are frequently used in phantoms designed to mimic the breast (11, 12). Further, iohexol was used to fill the pits of the first object and the cavities of the second object. Iohexol contrast is widely used in hospitals. Physical dimensions of both phantoms were similar to the dimensions of a compressed breast. Objects are displayed on Fig. 1.

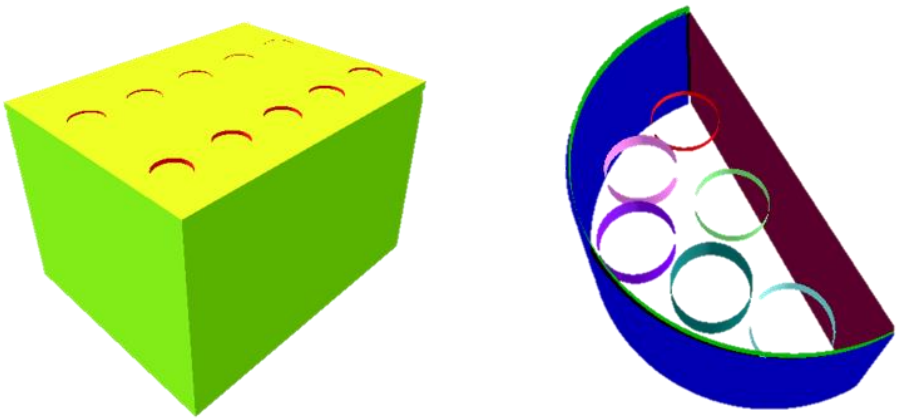

Figure 1. Computational phantoms created for the study: (left) first object: parallelepiped and (right) second object: semi cylinder.

Images: The basic geometric parameters of a radiology unit are the distances between the source and the isocenter, and the distance between the source and the detector. For the simulations, these distances were selected to be 1000 mm and 1300 mm, respectively. The simulated energy spectra are 50 kVp, 80 kVp, 100 kVp and 120 kVp. Their mean energies were used to model the x-ray images for each computational object. These x-ray images were processed for correspond to x-ray exposure of 1 mGy. Photon noise was added using equation (1):

$$N = N_0 e^{-\mu l} + \delta, \qquad \delta = \text{Poisson}(\sqrt{N}) \qquad (1)$$

where N and N_0 are the number of the photons passing through the object and number of the photons at the source respectively.

The subtraction method: The method used to subtract the images is based on the dual-energy algorithm, described in (13). Pixel-by-pixel weighted subtraction was applied by equation (2), where each image pixel value P_{SR} depends on the low energy noisy image pixel value P_L, the high energy noisy image pixel value P_H, and a coefficient w:

$$P_{SR} = P_L - w.P_H \qquad (2)$$

In calculations different values of w between 0 and 4 were tested and the best value was experimentally defined. For this purpose, two regions of interest (ROI) on each subtraction result image were defined: the first ROI was selected inside the area of the deepest iohexol pit for the images of the first object and highest iohexol cavity for the images of the second object, and the second ROI was selected in the area free of iodine-based contrast. Both ROI had dimensions 30 x 30 pixels. Next, we calculated average value for the respective ROI, calling them "signal value" (SV) for average values within the first ROI and "background value" (BV) for the average value within the second ROI. Finally, we calculated the contrast value (CV) for each subtraction result image using SV and BV for the respective image and the equation (3) (14):

$$CV = (SV-BV)/BV \qquad (3)$$

Thus, for each energy pair, we determined the weighted coefficient w that provided the highest contrast.

For comparison purposes, the theoretical weighted coefficients, w_c, were calculated by equation (4). These coefficients depend on low energy attenuation coefficient μ_L and high energy attenuation coefficient μ_H for each energy pair and each background material – clear resin or PMMA:

$$w_c = (\mu_L/ \mu_H) \qquad (4)$$

Results

Fig. 2 shows the simulated noisy x-ray images of the first computational object obtained at the four different incident energies, while Fig. 3 shows the noisy images of the second computational object for the same incident energies. As expected, the increase of the incident photon energy resulted in lower contrast images, which can be explained with the increased influence of the Compton scattering.

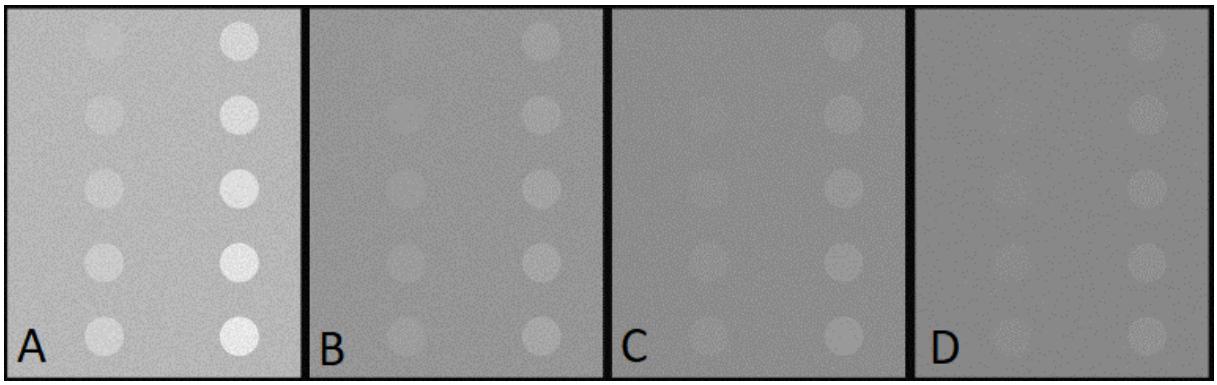

Figure 2. Simulated x-ray noisy images of the first object: (A) 50 kVp, (B) 80 kVp, (C) 100 kVp, (D) 120 kVp.

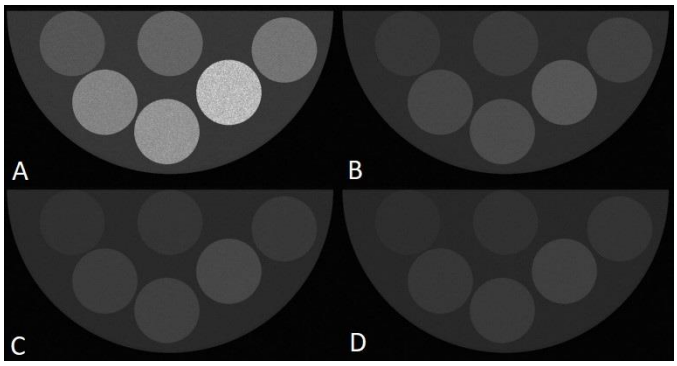

Figure 3. Simulated x-ray noisy images of the second object: (A) 50 kVp, (B) 80 kVp, (C) 100 kVp, (D) 120 kVp.

Table 1 displays the results for the weighted coefficients w and w_c, which correspond to the maximum contrast value (CV_{max}) for each energy pair for the first object, while Table 2 shows the respective data obtained for the second object.

Table 1. Weighted coefficients for the first object

energy pair	**low energy, kVp**	**high energy, kVp**	**weighted coefficient, theoretical, w_c**	**weighted coefficient, simulation, w**
1	50	80	1.233	1.244
2	50	100	1.314	1.319
3	50	120	1.367	1.377
4	80	100	1.065	1.060
5	80	120	1.109	1.106
6	100	120	1.040	1.044

Table 2. Weighted coefficients for the second object

energy pair	low energy, kVp	high energy, kVp	weighted coefficient, theoretical, wc	weighted coefficient, simulation, w
1	50	80	1.254	1.259
2	50	100	1.342	1.348
3	50	120	1.400	1.405
4	80	100	1.071	1.071
5	80	120	1.116	1.116
6	100	120	1.042	1.042

Comparing the theoretical values of w_c shown in Table 1 and Table 2 with calculated from the simulation w, it is seen that differences were small with the greatest of them 0.011 for the energy pair 1 for the first object. Generally, the differences for both objects were greater when the low energy was 50 kVp. Differences in the values of w and w_c were less for the second object. The explanation is that the deepest pit on the first object was 1 mm while the largest cavity of the second object had height 8 mm therefore it was more noise resistant.

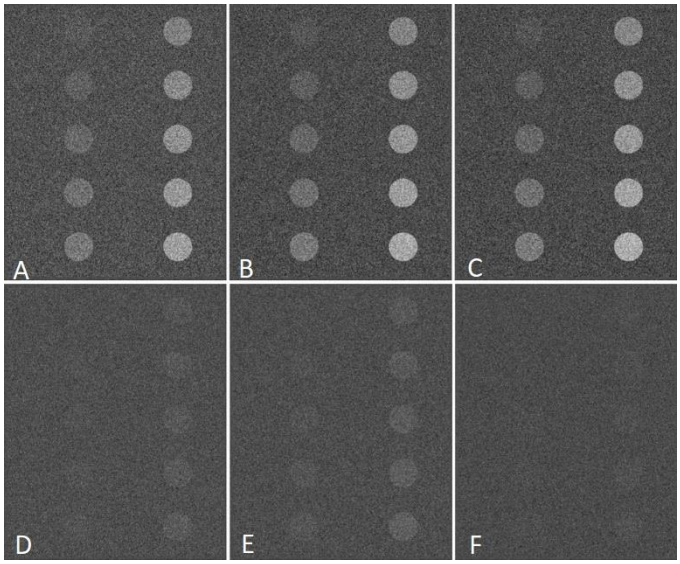

Figure 4. Subtraction result noisy images with best contrast for each of the energy pairs for the first object:
(A) pair 50 kVp – 80 kVp, (B) pair 50 kVp – 100 kVp, (C) pair 50 kVp – 120 kVp,
(D) pair 80 kVp – 100 kVp, (E) pair 80 kVp – 120 kVp, (F) pair 100 kVp – 120 kVp.

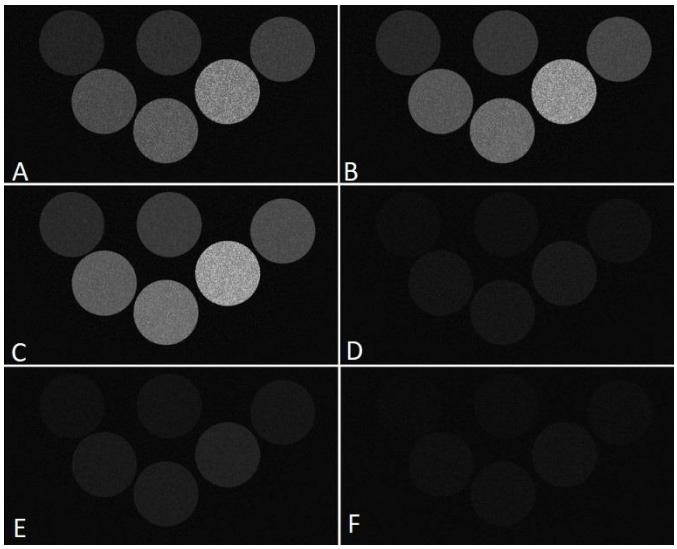

Figure 5. Subtraction result noisy images with best contrast for each of the energy pairs for the second object:
(A) pair 50 kVp – 80 kVp, (B) pair 50 kVp – 100 kVp, (C) pair 50 kVp – 120 kVp,
(D) pair 80 kVp – 100 kVp, (E) pair 80 kVp – 120 kVp, (F) pair 100 kVp – 120 kVp.

Fig. 4. displays subtraction images for the first object with values of w as listed in table I, while the subtraction result images for the second object with values for w listed in table II are displayed on Fig. 5. All images were visualized using ImageJ and images for each object had same settings.

Next steps are related to the experimental validation of the models: the acquisition of images and their subtracted image, as well as with further improvement of the subtraction algorithm.

Conclusions

This study established the background for performing simulated optimisation studies with contrast-enhanced imaging. Noisy x-ray images were successfully generated and suitably processed to obtain CEDEM images. Subtraction result images of energy pairs with 50 kVp as low energy had good contrast even for smaller quantities of iodine agent as in the case of the pits of the first object.

Acknowledgement

This project has received funding from the European Union's Horizon 2020 research and innovation programme under the Marie Skłodowska-Curie grant agreement No 101008020

References

1. American Cancer Society , Inc. https://canceratlas.cancer.org/the-burden/europe/
2. American College of Radiology. https://www.acr.org/-/media/ACR/Files/RADS/BI-RADS/Mammography-Reporting.pdf

3. Baldelli P, Bravin A, Di Maggio C, Gennaro G, et al., “Evaluation of the minimum iodine concentration for contrast-enhanced subtraction mammography”, Phys. Med. Biol. **51**, 2006, pp. 4233-4251. doi:10.1088/0031-9155/51/17/008

4. Dromain C, Balleyguier C, Adler G, Garbay JR, Delaloge S., “Contrast-enhanced digital mammography”, European Journal of Radiology, **69**, 2009, pp. 34-42. doi:10.1016/j.ejrad.2008.07.035

5. Dromain C, Thibault F, Muller S, Rimareix F, et al., “Dual-energy contrast-enhanced digital mammography: initial clinical results”. Eur. Radiol. **21**, 2011, pp. 565-574. doi: 10.1007/s00330-010-1944-y

6. Sung JS, Lebron L, Keating D, D’Alessio D, et al., “Performance of dual-energy contrast-enhanced digital mammography for screening women at increased risk of breast cancer”, Radiology, **293**, 2019, pp. 81-88. doi: 10.1148/radiol.2019182660

7. Xing D, Lv Y, Sun B, Xie H, et al., “Diagnostic value of Contrast-Enhanced Spectral Mammography in Comparison to Magnetic Resonance Imaging in Breast Lesions”, J Comput Assist Tomogr, **43**, 2019. pp 245-251. doi: 10.1097/RCT.0000000000000832

8. Steinhof-Radwanska K, Grazynska A, Barczyk-Gutkowska A, Kajor M, et al., “The new method, the old problem – role of contrast enhanced spectral mammography in the diagnosis of breast cancer among Polish women”, Pol J Radiol, **85**, 2020, pp.381-381. doi: 10.5114/pjr.2020.97941

9. Lorek A, Steinhof-Radwanska K, Barszyk-Gutkowska A, Zarebski W, et al., “The Usefulness of Spectral Mammography in Surgical Planning of Breast Cancer Treatment – Analysis of 999 Patients with Primary Operable Breast Cancer”, Curr. Oncol. **28**, 2021, pp. 2548-2559. doi: 10.3390/curroncol28040232

10. Bliznakova K, Speller R, Horrocks J, Liaparinos P, et al., “Experimental validation of a radiographic simulation code using breast phantom for x-ray imaging”, Comput Biol Med, **40**(2), 2010, pp.208-214. doi: 10.1016/j.compbiomed.2009.11.017

11. K. Bliznakova, “The advent of anthropomorphic three-dimensional breast phantoms for X-ray imaging”, Physica Medica, 2020 Nov;79. pp.145-161. doi: 10.1016/j.ejmp.2020.11.025

12. Marziani, M., Taibi A, Tuffanelli A, Gambaccini M., "Dual-energy tissue cancellation in mammography with quasi-monochromatic x-rays." Phys. Med. Biol. 2002 **47(2)**: pp. 305-313. doi: 10.1088/0031-9155/47/2/309

13. Bliznakova K, Kolitsi K, Pallikarakis N, “Dual-energy mammography: Simulation studies” Phys. Med. Biol. 2006, **51** (18) pp. 4497-4515. doi: 10.1088/0031-9155/51/18/004

14. “Webb’s physics of medical imaging” edited by M. A. Flower, CRC Press, 2012.